

## Article

# Estimating Corn Growth Parameters by Integrating Optical and Synthetic Aperture Radar Features into the Water Cloud Model

Yanyan Wang<sup>1,2</sup>, Zhaocong Wu<sup>1,\*</sup>, Shanjun Luo<sup>1,2</sup>, Xinyan Liu<sup>1,2</sup>, Shuaibing Liu<sup>2</sup> and Xinxin Huang<sup>3</sup>

<sup>1</sup> Aerospace Information Research Institute, Henan Academy of Sciences, Zhengzhou 450046, China; yyan@hnas.ac.cn (Y.W.); luoshanjun@hnas.ac.cn (S.L.); lxy\_rs@hnas.ac.cn (X.L.)

<sup>2</sup> School of Remote Sensing and Information Engineering, Wuhan University, Wuhan 430072, China; liushuaibing@whu.edu.cn

<sup>3</sup> School of Economics & Management, Northwest University, Xi'an 710127, China; huangxinxin@stumail.nwu.edu.cn

\* Correspondence: zcwoo@hnas.ac.cn

**Abstract:** Crop growth parameters are the basis for evaluation of crop growth status and crop yield. The aim of this study was to develop a more accurate estimation model for corn growth parameters combined with multispectral vegetation indexes ( $VI_{opt}$ ) and the differential radar information (DRI) derived from SAR data. Targeting the estimation of corn plant height (H) and the BBCH (Biologische Bundesanstalt, Bundessortenamt and CHEmical industry) phenological parameters, this study compared the estimation accuracies of various multispectral vegetation indexes ( $VI_{opt}$ ) and the corresponding  $VI_{DRI}$  (vegetation index corrected by DRI) indexes in inverting the corn growth parameters. (1) When comparing the estimation accuracies of four multispectral vegetation indexes (NDVI, NDVI<sub>re1</sub>, NDVI<sub>re2</sub>, and S2REP), NDVI showed the lowest estimation accuracy, with a normalized root mean square error (nRMSE) of 20.84% for the plant height, while S2REP showed the highest estimation accuracy (nRMSE = 16.05%). In addition, NDVI<sub>re2</sub> (nRMSE = 16.18%) and S2REP (16.05%) exhibited a higher accuracy than NDVI<sub>re1</sub> (nRMSE = 19.27%). Similarly, for BBCH, the nRMSEs of the four indexes were 24.17%, 22.49%, 17.04% and 16.60%, respectively. This confirmed that the multispectral vegetation indexes based on the red-edge bands were more sensitive to the growth parameters, especially for the Sentinel-2 red-edge 2 band. (2) The constructed  $VI_{DRI}$  indexes were more beneficial than the  $VI_{opt}$  indexes in enhancing the estimation accuracy of corn growth parameters. Specifically, the nRMSEs of the four  $VI_{DRI}$  indexes (NDVI<sub>DRI</sub>, NDVI<sub>re1DRI</sub>, NDVI<sub>re2DRI</sub>, and S2REP<sub>DRI</sub>) decreased to 19.64%, 18.11%, 15.00%, and 14.64% for plant height, and to 23.24%, 21.58%, 15.79%, and 15.91% for BBCH, indicating that even in cases of high vegetation coverage, the introduction of SAR DRI features can further improve the estimation accuracy of growth parameters. Our findings also demonstrated that the NDVI<sub>re2DRI</sub> and S2REP<sub>DRI</sub> indexes constructed using red-edge 2 band information of Sentinel-2 and SAR DRI features had more advantages in improving the estimation accuracy of corn growth parameters.

**Keywords:** red-edge vegetation index; DRI; plant height; BBCH



**Citation:** Wang, Y.; Wu, Z.; Luo, S.; Liu, X.; Liu, S.; Huang, X. Estimating Corn Growth Parameters by Integrating Optical and Synthetic Aperture Radar Features into the Water Cloud Model. *Agriculture* **2024**, *14*, 695. <https://doi.org/10.3390/agriculture14050695>

Academic Editor: Bruno Bernardi

Received: 22 February 2024

Revised: 22 April 2024

Accepted: 25 April 2024

Published: 28 April 2024



**Copyright:** © 2024 by the authors. Licensee MDPI, Basel, Switzerland. This article is an open access article distributed under the terms and conditions of the Creative Commons Attribution (CC BY) license (<https://creativecommons.org/licenses/by/4.0/>).

## 1. Introduction

Optical remote sensing images can obtain rich spectral features of vegetation canopy, especially the red-edge bands sensitive to green vegetation, which have absolute advantages for monitoring crop growth. However, optical remote sensing images are susceptible to weather conditions. It is often difficult to obtain satisfactory optical images during the cloudy and rainy season of crop growth. In view of this, some scholars have studied methods for monitoring crop growth based on time-series Synthetic Aperture Radar (SAR) images [1,2]. However, these methods require SAR images throughout the entire crop growth season, with a large data volume and complex data processing. Moreover, using SAR data alone cannot effectively utilize the rich spectral features of crop canopies

reflected by optical data. Therefore, removing the need for time-series SAR data, this study investigated a method for estimating corn growth parameters by combining multispectral and backscatter features based on partially obtainable optical and SAR data during the crop growth season.

Existing research has shown that there is a good correlation between the optical vegetation indexes and crop growth parameters [3,4]. However, when vegetation coverage or aboveground biomass is high, especially for corn crops with a large plant size, the optical vegetation indexes are more prone to saturation in the middle or later growth stages [5,6]. At this time, the optical vegetation indexes are less sensitive to the crop growth parameters. Some studies have found that there is a better correlation between the red-edge bands and the growth parameters of green vegetation. The red-edge vegetation indexes can weaken the saturation phenomenon to a certain extent when the vegetation coverage is high, and they can more effectively monitor the crop growth status and the growth parameters [7,8]. However, even the red-edge vegetation indexes, which are sensitive to crop growth changes, only reflect the spectral reflectance characteristics of the vegetation canopy and cannot reflect the internal structural characteristics of the crop canopy. In comparison, SAR signals are more sensitive to the internal structure and geometric characteristics of the crop due to their penetration ability [9,10], which to some extent compensates for the shortcomings of optical image data [11]. At present, there is still relatively little research on using complementary information from optical and SAR data to estimate crop growth parameters, but some progress has been made [12,13]. Luo et al. proposed a method that combined optical and SAR features to estimate the corn LAI (Leaf Area Index) and biomass parameters, and the results showed that combining spectral and texture features can significantly improve the estimation accuracy of the crop LAI and biomass [14]. Abdikan et al. verified the correlation between variables determined from Synthetic Aperture Radar (SAR) and optical images and the plant height of the sunflower [15]. Yeasin et al., based on machine learning models, examined whether combined Sentinel-1 and Sentinel-2 data are more efficient in predicting the sugarcane phenology than Sentinel-1 and Sentinel-2 data alone [16]. However, the current research based on the combination of these two different types of features is at the data level. There is little analysis of the different responses of optical and SAR features to crop growth parameters from a mechanistic level.

Radar vegetation scattering models describe the scattering mechanism of radar signals on vegetation-covered surfaces, and they accurately characterize the scattering and absorption characteristics of radar waves on these surfaces [17]. Among them, the Michigan Microwave Canopy Scattering (MIMICS) model is currently the most comprehensive vegetation scattering model, which has been used in the study of scattering characteristics of various vegetation types since its establishment [18,19]. However, the MIMICS model has a large number of input parameters, which to some extent affects the accuracy of vegetation scattering model construction and crop growth parameter estimation [20]. The Water Cloud Model (WCM), as one of the typical semi-empirical scattering models, does not require complex geometric mathematical models to describe the interaction between microwaves and vegetation. It is more general than empirical models and easier to use than physical models [21,22]. It has been widely used in the evaluation of vegetation growth parameters in recent years. Yang et al. used three scattering components obtained from polarization decomposition, coupling those with the modified WCM, and they estimated the rice LAI, plant height, and panicle biomass based on time-series RADARSAT-2 fully polarized SAR data throughout the entire growth cycle [23]. Kweon et al. improved the WCM based on corn and soybean crops by introducing the mean and standard deviation of crop canopy leaf inclination distribution, further enhancing the estimation accuracy of crop growth parameters based on the WCM [24]. In addition, Bai et al. proposed a soil moisture estimation method based on the WCM and the Advanced Integral Equation Model (AIEM), and they found that the method has the potential to estimate crop growth parameters [25]. These studies have verified that the scattering mechanism of radar waves over vegetation-covered

surfaces described by the WCM can effectively explain the scattering contribution of the vegetation layer and thus achieve growth parameter estimation for different crops.

Therefore, the aim of this study was to explore the combined method of using complementary optical and SAR information at the mechanistic level, and to construct a growth parameter estimation model suitable for the corn crop. Since the WCM is most suitable for describing the microwave scattering mechanism in areas with a relatively uniform vegetation cover [26,27], the optical and SAR satellite images selected in this paper were all in the late jointing or tasseling stages of the corn crop. At this time, the corn already has a large plant body size, and the ground is completely covered by the vegetation, meeting the condition that volume scattering dominates, which is in accordance with the principles of the WCM. In order to obtain a more accurate growth parameter estimation model, this study comprehensively utilized the advantages of optical and SAR data, combined with the principle of the WCM, without the need for other external data or a large volume of data. This approach led us to develop a new method that integrates multispectral vegetation indexes and differential radar information (DRI) features, achieving the high-precision estimation of crop growth parameters. In this paper, estimation models of field corn plant height and phenological stage parameters, respectively, are presented.

## 2. Materials and Methods

### 2.1. Experimental Area

The research area is located in Jiaozuo City, Henan Province, with the central coordinates of  $113^{\circ}23'$  E and  $35^{\circ}12'$  N. Jiaozuo is bordered by the Yellow River in the south and the Taihang Mountains in the north. It is one of the most famous grain-producing areas in China. This area is mainly planted with wheat, corn, soybeans, peanuts, potatoes, etc. The region has a temperate monsoon climate with four distinct seasons. The annual average temperature is  $13^{\circ}\text{C}$ , with January being the coldest month at an average temperature of  $0^{\circ}\text{C}$ , while July is the hottest with an average monthly temperature of  $28^{\circ}\text{C}$ . The annual precipitation in this area is about 600–1200 mm. The main agricultural planting mode is a winter wheat and summer corn rotation. Summer corn is usually sown as soon as possible after the winter wheat harvest in early June and harvested at the end of September, with the entire growth period lasting approximately 110 days. The locations of the experimental area and ground sampling points are shown in Figure 1.

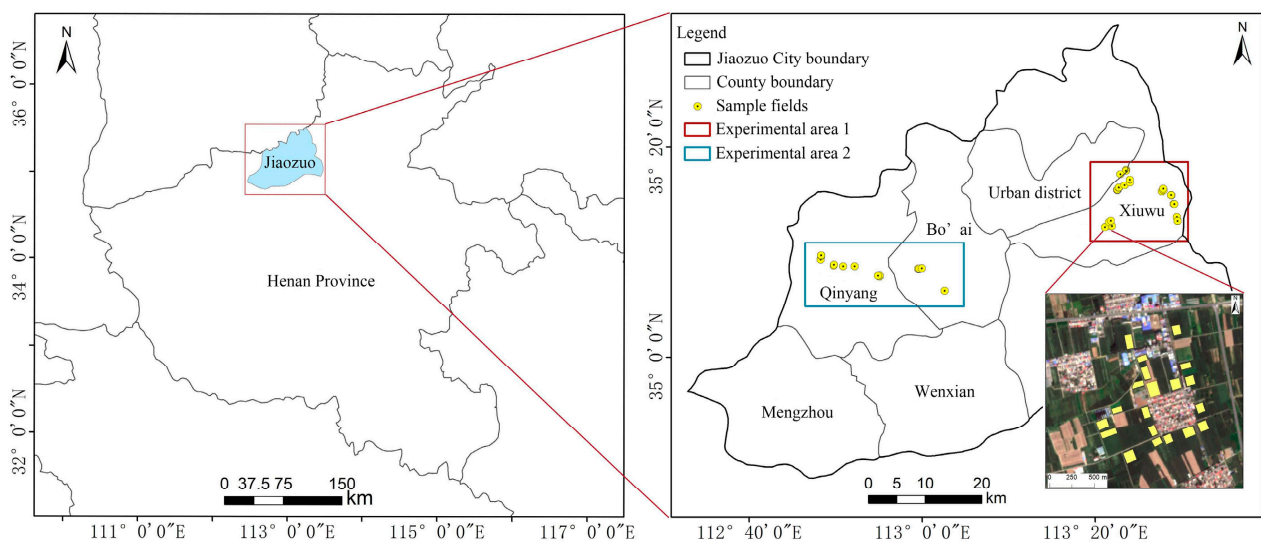


**Figure 1.** Location of the experimental areas and some ground sampling points (Yellow rectangles show the specific sampling fields).

The experimental area was divided into experimental area 1, located in Xiuwu County to the east of Jiaozuo City, and experimental area 2, located in Qinyang and Bo'ai Counties

to the west of Jiaozuo City. In the study area, experimental area 1 was covered by the 113 and 40 orbit data of the Sentinel-1 satellite, while only the 113 orbit data covered experimental area 2. Therefore, the Sentinel-1 SAR satellite data for experimental areas 1 and 2 had different measurement dates and radar incidence angles. Since the SAR data intensity is affected by the incidence angle, and the radar incidence angle varies greatly in different sample fields, especially when the satellite is in different orbits, the effect of the radar incidence angle could not be ignored in this study.

## 2.2. In Situ Data

The field investigation mainly measured and recorded the plant height and phenological stage information throughout the entire corn growth period in the study area in 2021. In that time, 39 sample fields were observed in experimental area 1, and 20 summer corn fields were observed in experimental area 2. The corn sample fields were planted in a family unit, so the corn plants in the same field had the same cultivated variety and field management level. All the corn fields were sown with a uniform seeder, with a row spacing of 60 cm and a plant spacing of 10–20 cm. The area of each field varied from 0.65 hectares to 1.94 hectares, with an average area of about 1.04 hectares. Before the field investigation, boundary information for each sample field was determined by combining a GPS locator and a Google Images map. The morphological characteristics and corresponding BBCH (Biologische Bundesanstalt, Bundessortenamt and CHEmical industry) codes [28] of the corn at different growth stages are shown in Table 1. The BBCH coding is a decimal system based on the well-known code for cereals developed by Zadoks et al., which makes it possible to unify the coding of all crops and weeds at the same physiological growth stage [29].

**Table 1.** Morphological characteristics and corresponding BBCH codes of corn at different growth stages.

No.	Phonology Stages	Morphological Characteristics	BBCH Code
1	Emergence	Expose the first leaf from the tooth sheath.	10
2	Three Leaves	Expose the third leaf from the second leaf sheath.	13
3	Seven Leaves	Expose the seventh leaf from the sixth leaf sheath.	17
4	Jointing	The round and hard stem nodes can be felt near the ground.	31
5	Tasseling	The top spikelet of the male spike protrudes from the leaf sheath.	51
6	Male florescence	The anthers in the upper part of the male spike are exposed, and pollen is scattered.	55
7	Silking	Floral filaments are exposed in the bracts of female spikes in plants.	61
8	Milk ripening	The shape of the grains has reached normal size, and the lower middle grains of the fruit inflorescence are filled with thick white milk.	79
9	Maturity	More than 80% of plants have yellowed outer bracts, dried filaments, and hardened grains.	89

The field investigation of corn phenological stages was carried out according to the Meteorological Industry Standard of the People’s Republic of China [30] and the record specification of the corn crop BBCH [28]. The field investigation of the phenological stages was carried out every other day. The stages of emergence, milky ripening, and maturity phenology were determined by visual discrimination. The other stages were determined by the percentage of the corn plants entering those phenological stages compared to the total number of observed plants. When the percentage was greater than or equal to 50%, this indicated that the field had entered the universal development period, and it was then that it was determined that the corn field had entered this phenological stage. For each sample field, 15–20 corn plants more than 2 m away from the edge of the plot were randomly selected for measurement and judgment.

The plant height was measured with a steel ruler from the root to the highest point of the canopy leaves in the natural state of the corn plant, or to the top of the male tassel after the tasseling stage. The unit of the measured plant height was in centimeters (cm), and the measurement data were rounded to an integer. For each sample field, 8 to 10 corn plants more than 2 m away from the edge of the plot were randomly selected for plant height measurement to obtain the plant height value of the field. In order to better match the ground measurement and satellite image data, and to reduce ground measurement errors, the ground measurement data were filtered and fitted based on logical functions, and they were interpolated with a daily interval. The fitting function is shown in Equation (1).

$$M = \frac{a}{1 + b \cdot \exp(ct)} \quad (1)$$

where  $M$  stands for the original field measurement data, natural constants  $a$ ,  $b$ , and  $c$  are function fitting parameters, and  $t$  is the date of the field investigation, represented here by DOY (day of year).

The original measurement data and corresponding fitted results of the plant height and BBCH for one of the sample fields are shown in Figure 2. The fitting function parameters of  $a$ ,  $b$ , and  $c$  for the plant height are 368.732,  $7.706 \times 10^9$ , and  $-0.116$ , respectively. For the BBCH, the fitting parameters are 101.430, 5368.613, and  $-0.040$ , respectively. In this study, the fitted results were used to represent the surface measurement data synchronized with satellite observations. The date of the surface measurement data was determined by the acquisition times of two optical satellite images. In this paper, the acquisition times of the two optical images were 26 July and 31 July 2021, respectively. Therefore, the fitted ground measurement data on these two days were extracted for estimation model construction and accuracy verification.

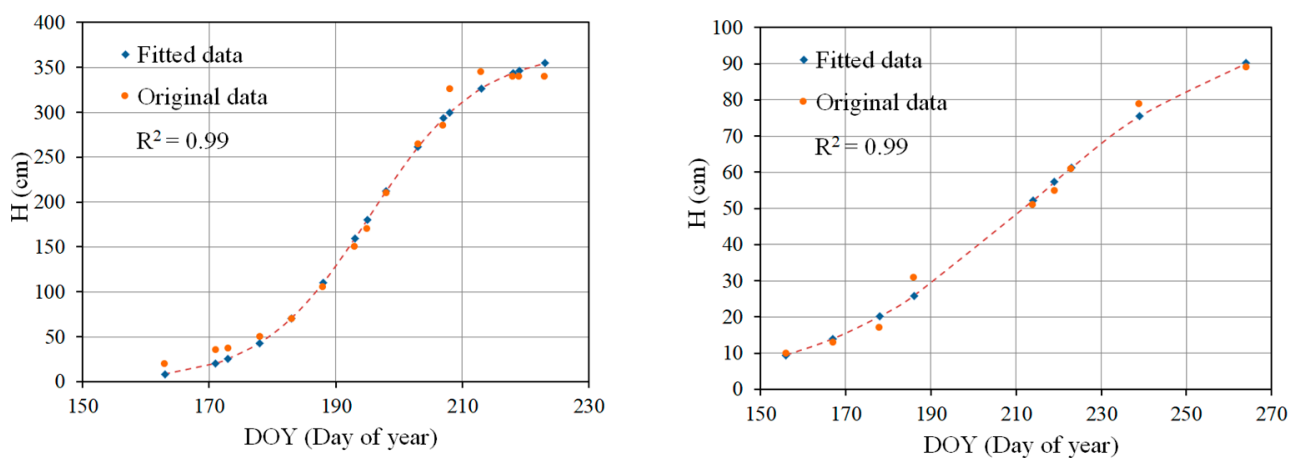


**Figure 2.** The original measured data (plant height and BBCH) and the corresponding logical fitting results (red dashed line represents the logistic fitting curve).

### 2.3. Image Data Collection

This study obtained synchronous optical and SAR satellite data covering two experimental areas. The detailed image parameters and coverage information are shown in Table 2. Among them, one SAR image acquired on August 1 and two optical images covered experimental area 1 and experimental area 2 at the same time. Due to differences in satellite orbits, the SAR images covering different experimental areas had significant differences in observation intervals and radar incidence angles. Therefore, experimental area 1 and experimental area 2 could be used as two independent experimental measurements for model training and verification, respectively. We trained the model based on the data of experimental area 1, and we used the data of experimental area 2 to further verify the accuracy and stability of the model.

The tasseling stage of the corn is an important turning point in its life. It is the transition period from plant vegetative growth to reproductive growth. At this time, all leaves of the corn have been expanded, the plant height or leaf area index (LAI) has reached the maximum; the plant body essentially stops vegetative growth and enters the stage centered on reproductive growth. The plant is very sensitive to the environmental conditions at this time. A continuous high temperature, drought, or rainy weather will directly affect the yield of the corn. Therefore timely and accurate monitoring of the growth status of corn crop in this phenological stage is necessary for timely guidance of field management and improvement of crop yield. Therefore, the images used in this study were mainly of the tasseling stage of corn.

**Table 2.** The detailed optical and SAR image parameters and coverage information.

Experimental	Types	Orbits	Platform	Acquisition Date	Phenology
area 1	Optical	/	Sentinel-2A	26 July 2021	Late jointing
	SAR	/	Sentinel-2B	31 July 2021	Tasseling
		40	Sentinel-1A	27 July 2021	Late jointing
		113	Sentinel-1A	1 August 2021	Tasseling
area 2	Optical	/	Sentinel-2A	26 July 2021	Late jointing
	SAR	/	Sentinel-2B	31 July 2021	Tasseling
		113	Sentinel-1A	1 August 2021	Tasseling
		113	Sentinel-1A	13 August 2021	Flowering

#### 2.4. Image Feature Extraction

From the Sentinel-1 SAR data, we mainly obtained the parameters of backscatter coefficient ( $\sigma_{VH}^0$  and  $\sigma_{VV}^0$ ) and radar incidence angle ( $\theta$ ). Firstly, in order to ensure that the backscatter coefficient from one image was not affected by the incidence angle, the radar incidence angle effect for each SAR image was normalized and corrected based on cosine normalization theory [31].

From the optical images, we mainly extracted multispectral vegetation indexes. The Sentinel-2 optical data used in this study contain three red-edge bands, which are sensitive to vegetation parameters. Therefore, the multispectral vegetation indexes of each sample field, mainly including the commonly used NDVI index [32], the normalized difference vegetation index NDVIre1 based on the red-edge 1 band [33], the normalized difference vegetation index NDVIre2 based on the red-edge 2 band [33], and the red-edge position index S2REP (Red-Edge Position Index, S2REP) specially designed by the ESA for Sentinel-2 [34], were calculated and extracted in this study.

#### 2.5. $VI_{DRI}$ Model Construction

Radar vegetation scattering models can describe a series of complex interactions between radar electromagnetic waves, various components of vegetation, and underlying surfaces. The main impact of vegetation on radar electromagnetic waves is the scattering and absorption of radar signals reaching the vegetation canopy. The scattering intensity of radar electromagnetic waves by vegetation is not only affected by the vegetation itself (the size and direction of scatterers in the vegetation canopy, the dielectric constant of the vegetation) but also by radar system parameters such as electromagnetic wave frequency, incidence angle, and polarization mode. The advantage of the WCM [35] is that the description of the scattering mechanism is relatively simple, and it can be used to describe scattering in areas with a relatively uniform vegetation coverage such as crop fields. However, the model ignores multiple scattering between vegetation and the underlying surface, and the prerequisite for applying this model is that the ground scattering mechanism is dominated by volume scattering. Therefore, when applied to sparse vegetation areas, it may lead to significant errors. However, the corn fields in this study were all in the late jointing or tasseling stages, meeting the condition that volume scattering dominated. Therefore, they were in accordance with the principles of the WCM. This study

introduced the application of the widely used Water Cloud Model (WCM) principle to corn growth monitoring.

According to the principle of the WCM [36], the total backscatter received by radar in a crop area is related to vegetation growth status (LAI, biomass, etc.) and underlying surface soil parameters (including the surface soil roughness and moisture). Therefore, directly using the original backscatter coefficient to invert vegetation growth parameters will result in significant errors. Meanwhile, the method of separating canopy and surface scattering terms through radar vegetation scattering models requires a large amount of surface measurement data input, which involves a huge workload for large-scale field crop growth parameters' estimation, and its accuracy is difficult to guarantee. Therefore, based on the WCM theory, combined with optical multispectral vegetation indexes and SAR differential radar information (DRI), the  $VI_{DRI}$  (vegetation index corrected by DRI) estimation model was constructed without the need for other external data inputs. The DRI represents the difference value of the backscattering coefficient between two SAR images, and the SAR data need to be synchronized with the optical images. The model establishment process was as follows:

$$\Delta\sigma^0 = \sigma_2^0 \left( \frac{\cos \theta_{norm}}{\cos \theta_2} \right) - \sigma_1^0 \left( \frac{\cos \theta_{norm}}{\cos \theta_1} \right) = \left( \frac{\sigma_2^0}{\cos \theta_2} - \frac{\sigma_1^0}{\cos \theta_1} \right) \quad (2)$$

$\theta_1, \theta_2$  is the radar incidence angle.  $\sigma_1^0, \sigma_2^0$  is the radar backscatter coefficient observed at different radar incidence angles in different observation times.  $\theta_{norm}$  is the parameter used to normalize the incidence angle. Firstly, the backscatter coefficients at different radar incidence angles are projected to a normal vector perpendicular to the ground surface. That is, the value of the  $\theta_{norm}$  parameter is set to 0 to normalize the effect of the incidence angle and unify the observation angle consistent with the optical remote sensing data. According to the principle of the WCM,  $\Delta\sigma^0$  can be expressed as follows:

$$\begin{aligned} \Delta\sigma^0 &= \Delta\sigma_{veg}^0 + (\tau_2^2 \sigma_{soil2}^0 - \tau_1^2 \sigma_{soil1}^0) \\ &= \Delta\sigma_{veg}^0 + [\tau_2^2 (C + Dm_2) - \tau_1^2 (C + Dm_1)] \end{aligned} \quad (3)$$

where  $\Delta\sigma^0$  describes the total difference value of the backscatter coefficient received by the SAR satellite during two observation intervals, including the VV and VH channels ( $\Delta\sigma_{VV}^0, \Delta\sigma_{VH}^0$ ).  $\Delta\sigma_{veg}^0$  represents the difference value of the backscatter coefficient from the crop vegetation layer.  $\sigma_{soil1}^0$  and  $\sigma_{soil2}^0$  represent the backscatter coefficient from the surface soil layer, and  $\tau_1^2$  and  $\tau_2^2$  are the two-way attenuation coefficient caused by the vegetation canopy.  $\Delta\sigma_{veg}^0$  and  $\tau_1^2, \tau_2^2$  are related to the growth status of crop vegetation, and  $\Delta\sigma_{veg}^0$  is positively correlated with the vegetation growth status, while  $\tau_1^2, \tau_2^2$  is negatively correlated with the growth status. Because the observation interval of two SAR images was short, and the corn plants had large body sizes and high vegetation coverage during these two periods, we considered  $\tau_1^2 \approx \tau_2^2 = \tau^2$ .  $\sigma_{soil1}^0$  and  $\sigma_{soil2}^0$  are related to the surface soil parameters and not the crop growth status. For two different observations of the same corn field, we assume that the soil roughness parameter C remains unchanged. Moreover, for the whole study area, we assume that the soil types and properties are essentially the same, and that the sensitivity parameter D related to the soil moisture content remains consistent. In addition, the changes in surface soil volume moisture contents of different fields within the same observation interval are thought to be similar, making  $\Delta m_v = m$ , at this time:

$$\begin{aligned} \Delta\sigma^0 &= \Delta\sigma_{veg}^0 + \tau^2 (\sigma_{soil2}^0 - \sigma_{soil1}^0) \\ &= \Delta\sigma_{veg}^0 + D\tau^2 [m_{v2} - m_{v1}] \\ &= \Delta\sigma_{veg}^0 + Dm\tau^2 \end{aligned} \quad (4)$$

where  $D$  and  $m$  are constants.  $\Delta\sigma^0$  is mainly related to  $\Delta\sigma^0_{\text{veg}}$  and  $\tau^2$ . Both  $\Delta\sigma^0_{\text{veg}}$  and  $\tau^2$  are a function of the parameters related to the vegetation layer in the WCM, and the value of these two parameters is related to the crop growth status. That is,  $\Delta\sigma^0$  of different fields calculated by differences weakens the influence of the surface roughness and surface soil moisture content on SAR data, and it can better reflect the growth status of the vegetation layer. Due to the close acquisition dates of the two SAR images, the plant height increment in these two periods was essentially the same. Therefore,  $\Delta\sigma^0$  reflects the variation characteristics of the radar backscatter coefficient under the same plant height increment of corn. Moreover, it shows the degree of complexity of the vegetation layer structure in the cross-section. The higher the value of  $\Delta\sigma^0$ , the more complex the structure of the vegetation layer in the unit cross-section, and the greater the LAI or biomass in the unit volume. Therefore, we introduce the parameter  $\Delta\sigma^0$  into the two-way attenuation  $\tau^2$  model. It can be expressed as follows:

$$\tau^2 = \exp(-2B \cdot V_2 / \cos \theta) = \exp(-2 \cdot \Delta\sigma^0) \quad (5)$$

In the WCM,  $\tau^2$  represents two-way attenuation of the radar signal by the vegetation layer.  $B$  represents the empirical coefficient, with a value depending on the crop type. Since this study only focused on the corn crop, here, it is defined as 1 to simplify the construction of the  $VI_{\text{DRI}}$  model.  $\theta$  is the radar incidence angle, and the incidence angle effect is considered in  $\Delta\sigma^0$  in this formula.  $V_2$  is a description of the vegetation canopy related to the crop growth status, which is generally expressed by parameters such as LAI or biomass of the vegetation. In the absence of ground-measured data, some scholars have introduced optical vegetation indexes related to the LAI or the biomass of the vegetation canopy to replace  $V_2$ . However, due to the limited penetration ability of optical data, optical vegetation indexes only reflect the spectral reflectance characteristics of the top of the vegetation canopy. For a corn crop with a large plant size,  $\Delta\sigma^0$  can better reflect the internal structural characteristics of the vegetation canopy than optical vegetation indexes. Therefore, this study used  $\Delta\sigma^0$  to replace  $V_2$ . The basic  $VI_{\text{DRI}}$  estimation model combining optical and SAR parameters was established as follows:

$$VI_{\text{DRI}} = \frac{VI_{\text{opt}}}{\tau^2_{\text{DRI}}} = \frac{VI_{\text{opt}}}{\exp(-2 \cdot \Delta\sigma^0)} \quad (6)$$

where  $VI_{\text{opt}}$  represents a multispectral vegetation index extracted from the optical data, such as the NDVI, NDVI<sub>re1</sub>, NDVI<sub>re2</sub>, or S2REP, which was correlated with the crop growth state due to the influence of the chlorophyll content of the vegetation.  $\tau^2_{\text{DRI}}$  represents the two-way attenuation coefficient of the crop and the radar wave described by the DRI, and the value of  $\tau^2_{\text{DRI}}$  ranges from 0 to 1. With the continuous growth of the crop, the attenuation effect of vegetation on the radar wave gradually increases, meaning the value of  $\tau^2_{\text{DRI}}$  gradually decreases. That is,  $\tau^2_{\text{DRI}}$  is negatively correlated with the crop growth state, and the newly established  $VI_{\text{DRI}}$  parameter is positively correlated with the vegetation growth state of corn. The whole technical process mainly includes data preprocessing, image features construction and growth parameters estimation, as shown in Figure 3.

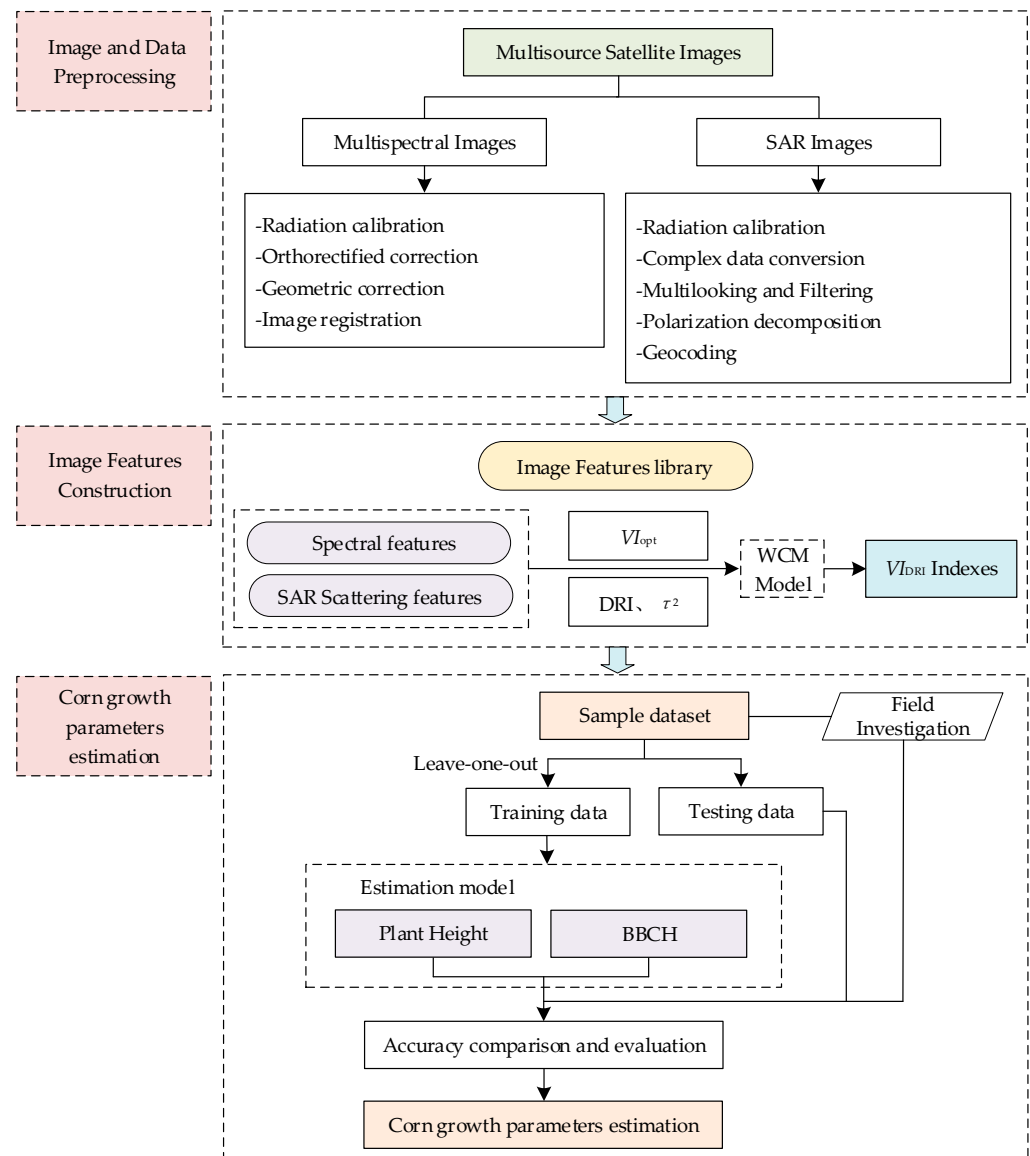


**Figure 3.** Flow chart of corn growth parameters estimation combined with multispectral and SAR features.

### 3. Results

#### 3.1. Correlation Analysis

In order to verify the superiority of the constructed  $VI_{DRI}$  indexes in estimating corn growth parameters (plant height and BBCH), the Pearson correlation ( $R$ ) between the vegetation indexes ( $VI_{opt}$  and  $VI_{DRI}$ ) and the plant growth parameters (plant height and BBCH) was analyzed by using the modeling data from experimental area 1, as shown in Table 3 and Figures 4 and 5.

**Table 3.** Pearson Correlation ( $R$ ) between the vegetation indexes and the growth parameters (plant height and BBCH).

$VI_{opt}$	Plant Height	BBCH	$VI_{DRI}$	Plant Height	BBCH
NDVI	0.35	0.08	$NDVI_{DRI}$	0.47	0.28
NDVire1	0.50	0.37	$NDVire1_{DRI}$	0.58	0.45
NDVire2	0.69	0.71	$NDVire2_{DRI}$	0.74	0.75
S2REP	0.69	0.72	$S2REP_{DRI}$	0.75	0.75

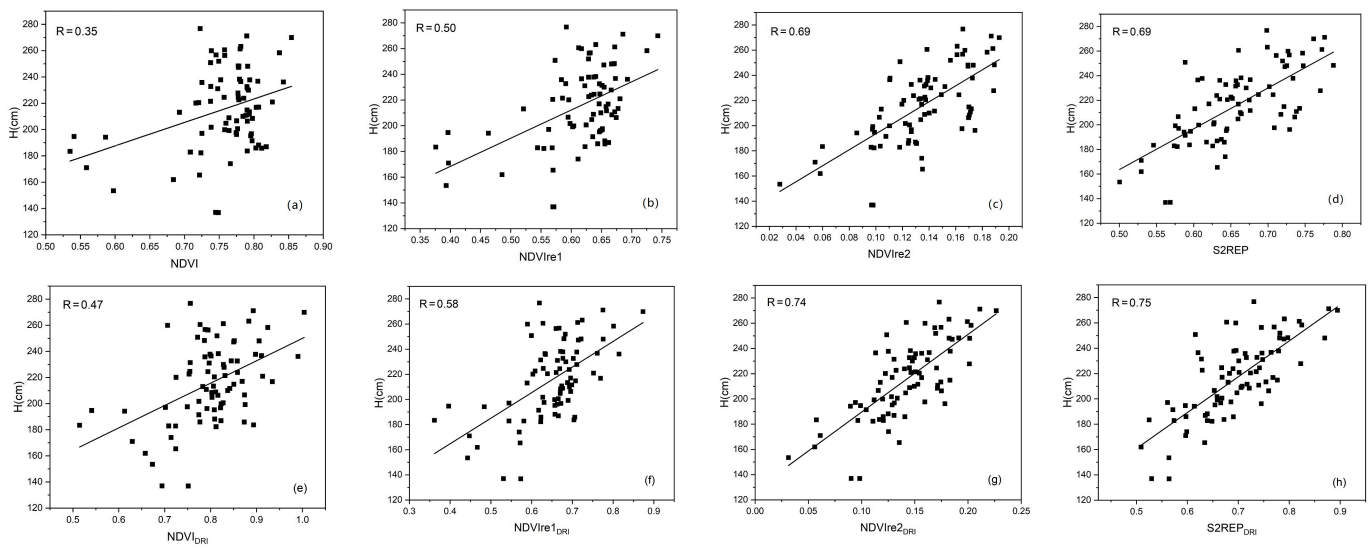


**Figure 4.** Scatter plot of  $VI_{opt}$  and corresponding  $VI_{DRI}$  indexes with plant height (NDVI, NDVIre1, NDVIre2 and S2REP are multispectral vegetation indexes.  $NDVI_{DRI}$ ,  $NDVIre1_{DRI}$ ,  $NDVIre2_{DRI}$  and  $S2REP_{DRI}$  are the corresponding  $VI_{DRI}$  indexes.  $H$  and  $R$  represents the plant height and Pearson Correlation, respectively. (a–d) represent the relationship between the plant height and the multispectral vegetation indexes. (e–h) represent the relationship between the plant height and the corresponding  $VI_{DRI}$  indexes. Black lines represent the linear fitting results).

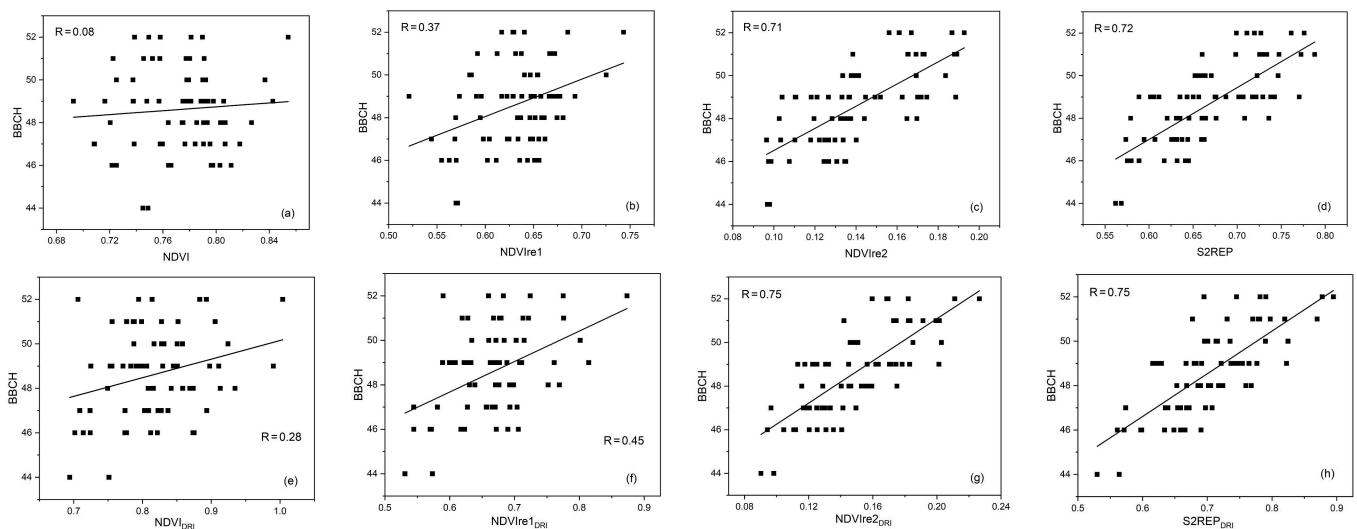


**Figure 5.** Scatter plot of  $VI_{opt}$  and corresponding  $VI_{DRI}$  indexes with BBCH (NDVI, NDVIre1, NDVIre2 and S2REP are multispectral vegetation indexes.  $NDVI_{DRI}$ ,  $NDVIre1_{DRI}$ ,  $NDVIre2_{DRI}$  and  $S2REP_{DRI}$  are the corresponding  $VI_{DRI}$  indexes. BBCH and  $R$  represents the phenology stage and Pearson Correlation, respectively. (a–d) represent the relationship between the BBCH and the multispectral vegetation indexes. (e–h) represent the relationship between the BBCH and the corresponding  $VI_{DRI}$  indexes. Black lines represent the linear fitting results).

Firstly, for the plant height, the  $VI_{DRI}$  constructed by introducing radar DRI could effectively improve the sensitivity of the multispectral vegetation indexes  $VI_{opt}$  to the change in the corn plant height. The Pearson correlation coefficients ( $R$ ) between the measured plant height and the NDVI, NDVIre1, NDVIre2, and S2REP were 0.35, 0.50, 0.69, and 0.69, respectively. Compared with the four  $VI_{opt}$  indexes, the correlation between the NDVI and the measured plant height was the lowest ( $R = 0.35$ ), which indicated that the  $VI_{opt}$  based on the red-edge band was more sensitive to the growth change in crops, especially

for NDVI<sub>re2</sub> and S2REP with the red-edge 2 band, where the correlation coefficient with plant height could reach 0.69. According to the scatter plot in Figure 4, the value of NDVI from the corn canopy in the experimental area was generally above 0.7, and showed a serious saturation phenomenon ( $R = 0.35$ ) in this situation, while NDVI<sub>DRI</sub> weakened this saturation phenomenon to some extent ( $R = 0.47$ ). In addition, NDVI<sub>re2</sub> and S2REP calculated by introducing the red-edge 2 band showed better correlations with plant height than NDVI<sub>re1</sub> calculated by introducing the red-edge 1 band. This verified the advantages of the Sentinel-2 red-edge 2 band in monitoring vegetation growth. In addition, compared with the four constructed VI<sub>DRI</sub> indexes, the correlation coefficients between NDVI<sub>DRI</sub>, NDVI<sub>re1DRI</sub>, NDVI<sub>re2DRI</sub>, and S2REP<sub>DRI</sub> and the measured plant height were 0.47, 0.58, 0.74, and 0.75, respectively. Among them, the correlation between NDVI<sub>DRI</sub> and the measured plant height was the lowest ( $R = 0.47$ ), while S2REP<sub>DRI</sub> calculated by introducing the red-edge 2 band had the highest correlation with plant height ( $R = 0.75$ ). Essentially, the VI<sub>DRI</sub> indexes constructed by introducing radar DRI showed higher correlations with plant height than using the multispectral vegetation indexes VI<sub>opt</sub> alone.

As for the BBCH, according to the scatter plot in Figure 5, the correlation coefficients between the measured BBCH and the NDVI, NDVI<sub>re1</sub>, NDVI<sub>re2</sub>, and S2REP were 0.08, 0.37, 0.71, and 0.72, respectively. It can be seen that the high vegetation coverage of the canopy makes it difficult to distinguish different phenological periods of corn just based on NDVI features. Among them, the correlation between the NDVI and the measured BBCH was the lowest ( $R = 0.08$ ), showing a complete saturation phenomenon. However, the correlation coefficients between the indexes of NDVI<sub>re2</sub> and S2REP constructed from the red-edge 2 band and BBCH reached 0.71 and 0.72, respectively. The correlation was much better than NDVI<sub>re1</sub> constructed from the red-edge 1 band ( $R = 0.37$ ), indicating that the multispectral indexes based on the red-edge 2 band are more sensitive to the corn BBCH than those based on the red-edge 1 band. Further comparison of the Pearson correlation coefficients ( $R$ ) between the measured BBCH and the constructed VI<sub>DRI</sub> revealed that the correlation coefficients between NDVI<sub>DRI</sub>, NDVI<sub>re1DRI</sub>, NDVI<sub>re2DRI</sub>, and S2REP<sub>DRI</sub> and the measured BBCH of corn were 0.28, 0.45, 0.75, and 0.75, respectively. Among them, NDVI<sub>DRI</sub> had the lowest correlation with the measured BBCH ( $R = 0.28$ ). Essentially, the introduction of red-edge multispectral features or SAR features to some extent improved the sensitivity of the vegetation indexes to the BBCH. In particular, NDVI<sub>re2DRI</sub> and S2REP<sub>DRI</sub> constructed by introducing the red-edge 2 band and DRI features showed the best correlations with BBCH ( $R = 0.75$ ). Similar to the plant height estimation, the introduction of radar DRI when constructing each VI<sub>DRI</sub> index could effectively enhance the sensitivity of VI<sub>opt</sub> to the BBCH. The results indicated that the VI<sub>DRI</sub> indexes combined with optical and SAR data also have certain advantages in improving the accuracy of corn BBCH estimation.

### 3.2. Estimation Model and Accuracy

In order to compare and analyze the accuracy of VI<sub>opt</sub> and its corresponding VI<sub>DRI</sub> indexes in estimating corn plant height and BBCH parameters, a simple linear regression equation determined by least squares combined with the Leave-One-Out cross-validation method was used to establish the estimation models of plant height and BBCH, respectively. We used the coefficient of determination ( $R^2$ ), root mean square error (RMSE), and normalized root mean square error (nRMSE) to analyze the performance of each regression model. Finally, combined with the field investigation data, a total of 78 iterations were carried out for the two periods of measurement data of 39 sample fields for experimental area 1. Tables 4 and 5 and Figures 6 and 7 show the estimation model and the model accuracy for the plant height and BBCH parameters from experimental area 1.

Table 4 shows the corn plant height estimation model and accuracy based on the multispectral vegetation indexes VI<sub>opt</sub> and the corresponding VI<sub>DRI</sub> indexes in experimental area 1. Essentially, the VI<sub>DRI</sub> indexes show higher estimation accuracy than the VI<sub>opt</sub> indexes. According to Figure 6a–d, comparing the corn plant heights estimated by four multispectral vegetation indexes NDVI, NDVI<sub>re1</sub>, NDVI<sub>re2</sub>, and S2REP,

whether for  $R^2$ , RMSE, or nRMSE, NDVI shows the lowest estimation accuracy ( $R^2 = 0.12$ , RMSE = 29.15, nRMSE = 20.84%), and S2REP shows the highest estimation accuracy ( $R^2 = 0.48$ , RMSE = 22.45, nRMSE = 16.05%). NDVIre1 has a limited ability to improve the accuracy of corn plant height estimation based on NDVI, while NDVIre2 and S2REP constructed with the red-edge 2 band have more advantages in improving the accuracy of the NDVI estimation model. This further verifies that the red-edge 2 band of Sentinel-2 data is more sensitive than the red-edge 1 band to crop height variation. In Figure 6e–h, the  $VI_{DRI}$  indexes corresponding to each multispectral vegetation index are compared and analyzed.  $NDVI_{DRI}$  shows the lowest model estimation accuracy ( $R^2 = 0.22$ , RMSE = 27.47, nRMSE = 19.64%), while  $S2REP_{DRI}$  shows the highest model estimation accuracy ( $R^2 = 0.57$ , RMSE = 20.48, nRMSE = 14.64%). Essentially, the  $VI_{DRI}$  indexes uniformly improve the accuracy of using  $VI_{opt}$  indexes to estimate the corn plant height. According to the scatter plots of corn plant height estimated by various vegetation indexes ( $VI_{opt}$  and  $VI_{DRI}$ ), as shown in Figure 6, during the tasseling stage of corn, high vegetation coverage leads to a severe saturation phenomenon of corn plant height estimation results based on the NDVI and NDVIre1 indexes. Meanwhile, NDVIre2 and S2REP significantly weaken this phenomenon, especially the  $NDVIre2_{DRI}$  and  $S2REP_{DRI}$  indexes constructed by further introducing radar DRI. All of these results verify that the combination of an optical red-edge band and radar DRI feature may effectively improve the plant height estimation accuracy for corn even under a high vegetation coverage condition.

**Table 4.** Plant height estimation model and accuracy based on the data from experimental area 1.

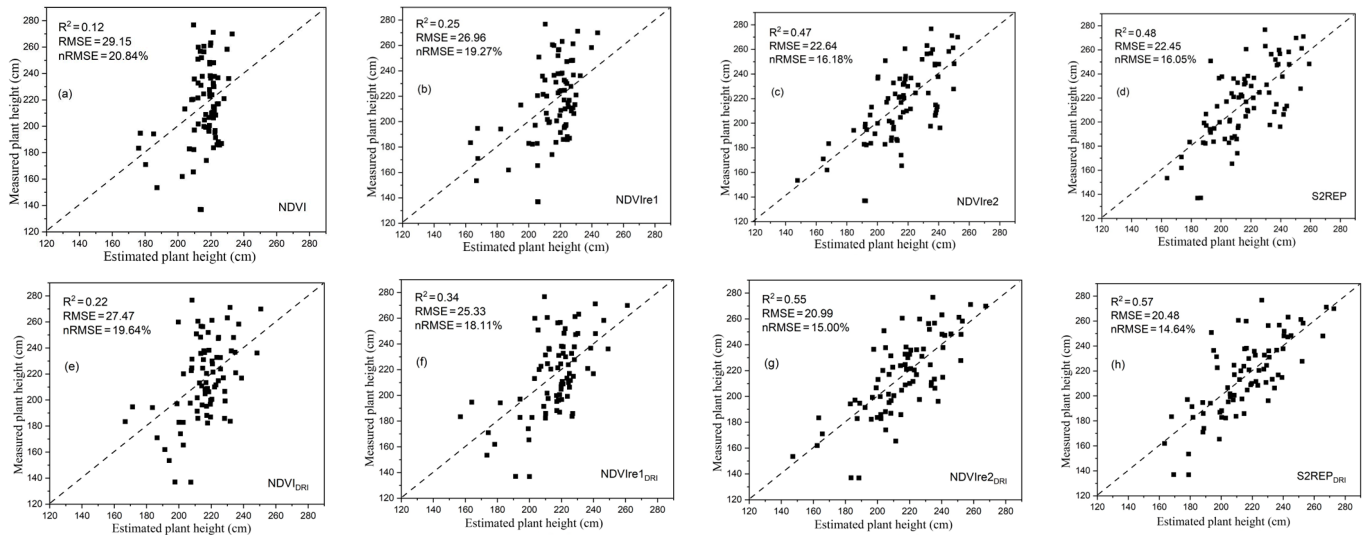
VI Types	VIs	Models	$R^2$	RMSE (cm)	nRMSE
$VI_{opt}$	NDVI	$y = 178.13x + 80.74$	0.12	29.15	20.84%
	NDVIre1	$y = 219.38x + 80.63$	0.25	26.96	19.27%
	NDVIre2	$y = 635.14x + 130.06$	0.47	22.64	16.18%
	S2REP	$y = 331.55x - 2.14$	0.48	22.45	16.05%
$VI_{DRI}$	$NDVI_{DRI}$	$y = 171.42x + 78.57$	0.22	27.47	19.64%
	$NDVIre1_{DRI}$	$y = 203.65x + 83.28$	0.34	25.33	18.11%
	$NDVIre2_{DRI}$	$y = 616.50x + 127.89$	0.55	20.99	15.00%
	$S2REP_{DRI}$	$y = 283.30x + 19.20$	0.57	20.48	14.64%

**Table 5.** BBCH estimation model and accuracy based on the data from experimental area 1.

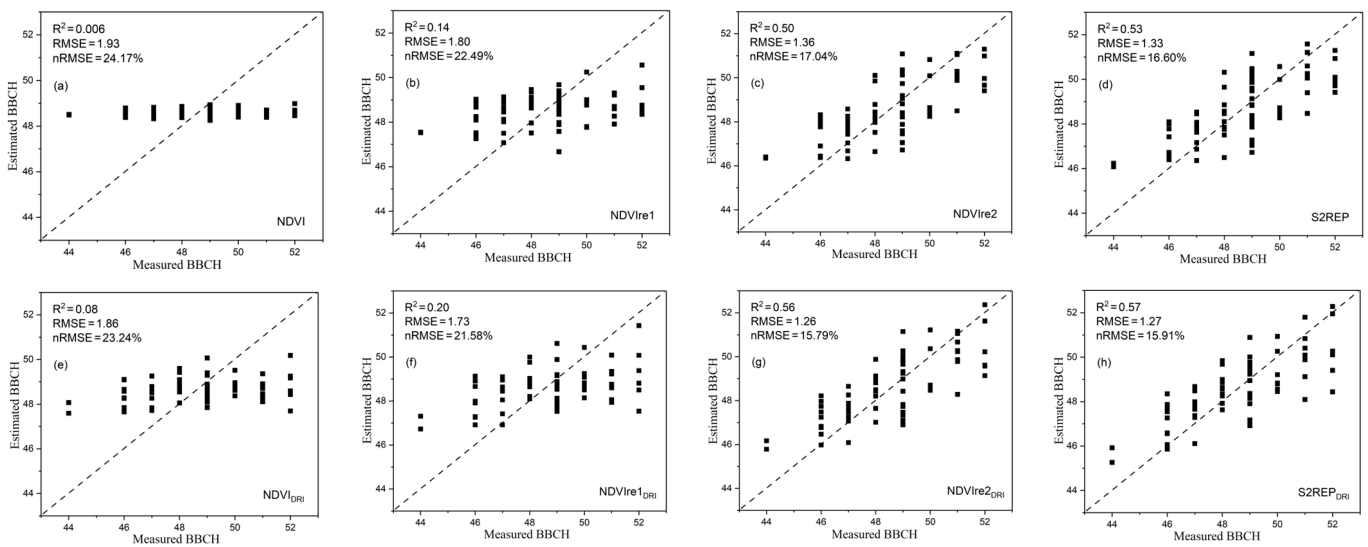
VI Types	VIs	Models	$R^2$	RMSE (cm)	nRMSE
$VI_{opt}$	NDVI	$y = 4.55x + 45.10$	0.006	1.93	24.17%
	NDVIre1	$y = 17.51x + 37.55$	0.14	1.80	22.49%
	NDVIre2	$y = 51.64x + 41.35$	0.50	1.36	17.04%
	S2REP	$y = 24.36x + 32.39$	0.53	1.33	16.60%
$VI_{DRI}$	$NDVI_{DRI}$	$y = 8.36x + 41.79$	0.08	1.86	23.24%
	$NDVIre1_{DRI}$	$y = 13.72x + 39.44$	0.20	1.73	21.58%
	$NDVIre2_{DRI}$	$y = 48.30x + 41.43$	0.56	1.26	15.79%
	$S2REP_{DRI}$	$y = 19.24x + 35.07$	0.57	1.27	15.91%

Table 5 shows the corn phenological stage (BBCH) estimation models and accuracies based on the multispectral vegetation indexes  $VI_{opt}$  and the corresponding  $VI_{DRI}$  indexes in experimental area 1. The same as the plant height estimation results, the  $VI_{DRI}$  indexes show a higher estimation accuracy than the  $VI_{opt}$  indexes. According to Figure 7a–d, when comparing the BBCH estimation results by the four multispectral vegetation indexes NDVI, NDVIre1, NDVIre2, and S2REP with the measured BBCH data on the ground, it can be seen that the NDVI shows the lowest accuracy of BBCH estimation results ( $R^2 = 0.006$ , RMSE = 1.93, nRMSE = 24.17%) with a serious saturation phenomenon. Meanwhile, NDVIre2 and S2REP have an obvious effect on weakening the saturation phenomenon, and the improvement effect is far better than with NDVIre1. This indicates that the red-edge 2 band of Sentinel-2 was more sensitive to the variation in the corn BBCH than the red-edge

1 band. According to Figure 7e–h, essentially, the  $VI_{DRI}$  indexes show a higher BBCH estimation accuracy than the  $VI_{Opt}$  indexes. Among them,  $NDVI_{DRI}$  shows the lowest BBCH estimation accuracy ( $R^2 = 0.08$ ,  $RMSE = 1.86$ ,  $nRMSE = 23.24\%$ ), while the  $S2REP_{DRI}$  index constructed by combining the Sentinel-2 red-edge 2 band and radar DRI shows the highest accuracy ( $R^2 = 0.57$ ,  $RMSE = 1.27$ ,  $nRMSE = 15.91\%$ ), which further verifies that the combination of an optical red-edge band and radar DRI feature can effectively improve the BBCH estimation accuracy for corn even under a high vegetation coverage condition.



**Figure 6.** Estimated plant height and measured plant height results based on the data from experimental area 1 ((a–d) represent the plant height estimation results using the NDVI, NDVIre1, NDVIre2, S2REP. (e–h) represent the plant height estimation results using the corresponding  $VI_{DRI}$  indexes, respectively. Dashed line represents a 1:1 relationship line).



**Figure 7.** Estimated BBCH and measured BBCH results based on the data from experimental area 1 ((a–d) represent the BBCH estimation results using the NDVI, NDVIre1, NDVIre2, S2REP. (e–h) represent the BBCH estimation results using the corresponding  $VI_{DRI}$  indexes, respectively. Dashed line represents a 1:1 relationship line).

In addition, we compared and analyzed the accuracy of NDVIre2, S2REP, and the corresponding  $NDVIre2_{DRI}$  and  $S2REP_{DRI}$  parameters, which were highly correlated with the growth status of corn, in estimating the plant height and the BBCH parameters. For the plant height, the accuracy of  $R^2$  and  $nRMSE$  based on  $NDVIre2_{DRI}$  increased by 0.08 and

1.18% compared to NDVI<sub>re2</sub>, and the accuracy ( $R^2$ , nRMSE) based on the S2REP<sub>DRI</sub> indexes increased by 0.09 and 1.41% compared to S2REP. For the estimation of BBCH, the accuracy ( $R^2$ , nRMSE) based on NDVI<sub>re2DRI</sub> increased by 0.06 and 1.25% compared to NDVI<sub>re2</sub>, and the accuracy ( $R^2$ , nRMSE) based on S2REP<sub>DRI</sub> increased by 0.04 and 0.69% compared to S2REP. This indicated that introducing radar DRI could better improve the accuracy of corn plant height estimation compared to BBCH. Through further analysis, it was found that the plant height reflects the characteristics of the crop in the vertical direction. Meanwhile, the BBCH difference of corn entering the tasseling stage is mainly reflected in the tassel extraction situation in the vegetation canopy, which shows the two-dimensional plane changes at the top of the crop canopy. Meanwhile, due to a certain penetrability, the SAR data can provide vertical structural information for the crop. Therefore, NDVI<sub>re2DRI</sub> and S2REP<sub>DRI</sub> are superior in improving the estimation accuracy for the corn plant height parameter compared to the BBCH.

### 3.3. Accuracy Verification

In order to further verify the superiority of the  $VI_{DRI}$  indexes in estimating the corn plant height and BBCH, and to test the accuracy of the estimation model in Tables 4 and 5, the NDVI<sub>re2</sub> and S2REP, as well as the corresponding  $VI_{DRI}$  indexes, which were sensitive to plant height and BBCH, were directly selected for comparative verification based on experimental area 2. The validation results and the accuracies are shown in Table 6 and Figure 8.

**Table 6.** Further accuracy verification of the estimation model based on the data from experimental area 2.

Parameters	VI Types	VIs	Models	$R^2$	RMSE (cm)	nRMSE
Plant height	$VI_{opt}$	NDVI <sub>re2</sub>	$y = 1078.6x + 62.80$	0.52	28.38	15.42%
		S2REP	$y = 531.55x - 140.36$	0.59	26.31	14.30%
	$VI_{DRI}$	NDVI <sub>re2DRI</sub>	$y = 1072.6x + 64.47$	0.55	27.28	14.83%
		S2REP <sub>DRI</sub>	$y = 505.89x - 121.17$	0.63	25.51	13.86%
BBCH	$VI_{opt}$	NDVI <sub>re2</sub>	$y = 45.40x + 40.97$	0.49	1.29	16.12%
		S2REP	$y = 23.23x + 31.84$	0.59	1.15	14.37%
	$VI_{DRI}$	NDVI <sub>re2DRI</sub>	$y = 45.44x + 41.00$	0.52	1.25	15.62%
		S2REP <sub>DRI</sub>	$y = 22.27x + 32.57$	0.64	1.09	13.62%

Table 6 and Figure 8 show the plant height and BBCH estimation models and accuracies based on NDVI<sub>re2</sub>, S2REP, and the corresponding  $VI_{DRI}$  indexes, which are sensitive to the corn growth parameters, using the data from experimental area 2. Essentially, the  $VI_{DRI}$  indexes constructed by combining optical and SAR data information show higher estimation accuracies than the optical vegetation indexes. However, different from experimental area 1, the constructed  $VI_{DRI}$  indexes used in experimental area 2 are relatively poor in improving the  $VI_{opt}$  indexes' estimation accuracy. This is because of the long interval between the two SAR images used in experimental area 2 and the poor synchronization with the optical images. Compared with the estimation results in Figures 6 and 8, for experimental area 1, the plant height estimation accuracy of  $R^2$  and nRMSE based on NDVI<sub>re2DRI</sub> increased by 0.08 and 1.18% compared to NDVI<sub>re2</sub>, and the plant height estimation accuracy ( $R^2$ , nRMSE) based on the S2REP<sub>DRI</sub> indexes increased by 0.09 and 1.41% compared to S2REP. However, in experimental area 2, the accuracy of  $R^2$  and nRMSE based on NDVI<sub>re2DRI</sub> increased by 0.03 and 0.55% compared to NDVI<sub>re2</sub>, and the accuracy ( $R^2$ , nRMSE) based on S2REP<sub>DRI</sub> increased by 0.04 and 0.44% compared to S2REP. As for the BBCH parameter, compared to the results in Figures 7 and 8, for experimental area 1, the BBCH estimation accuracy of  $R^2$  and nRMSE based on NDVI<sub>re2DRI</sub> increased by 0.06 and 1.25% compared to NDVI<sub>re2</sub>, and the estimation accuracy ( $R^2$ , nRMSE) based on the S2REP<sub>DRI</sub> indexes increased by 0.04 and 0.69% compared to S2REP. However, in experimental area 2, the accuracy of  $R^2$  and nRMSE based on NDVI<sub>re2DRI</sub> increased by 0.03 and 0.5% compared to NDVI<sub>re2</sub>, and the accuracy ( $R^2$ , nRMSE) based on the S2REP<sub>DRI</sub>

indexes increased by 0.05 and 0.75% compared to S2REP. That is, the constructed  $VI_{DRI}$  indexes used in experimental area 2 are relatively poor in improving the accuracy of using  $VI_{opt}$  indexes alone to estimate the crop growth parameter. The findings further indicate that a larger SAR data interval will reduce the  $VI_{DRI}$  indexes' ability to improve the estimation accuracy of corn growth parameters using the  $VI_{opt}$  indexes alone. In practice, the two SAR datasets used to calculate the DRI should be synchronized with the optical satellite data as much as possible, and the image time interval should not be too large.

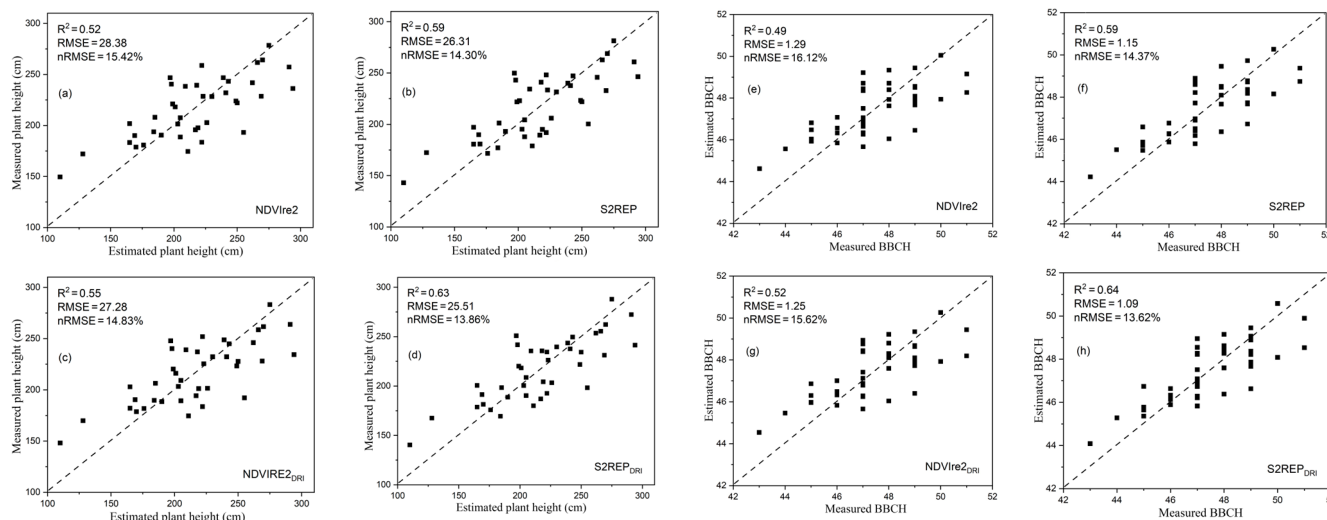


**Figure 8.** Estimated (plant height and BBCH) and measured (plant height and BBCH) results based on the data from experimental area 2 ((a–d) represent the plant height estimation results, (e–h) represent the BBCH estimation results using the NDVire2, S2REP NDVire2<sub>DRI</sub> and S2REP<sub>DRI</sub> indexes, respectively. Dashed line represents a 1:1 relationship line).

#### 4. Discussion

Optical satellite sensors have developed rapidly in recent years, with the advantages of low cost and high accuracy. Multispectral remote sensing data have a unique advantage in crop growth monitoring due to their rich spectral reflectance characteristics. The existing research has shown that the optical vegetation indexes are highly related to the aboveground biomass, LAI, vegetation coverage, etc., of crops [37]. However, the optical vegetation indexes are always sensitive to low vegetation coverage, and there is a serious saturation phenomenon when the vegetation coverage is medium to high [5,6]. In recent years, scholars have discovered important spectral bands, which are highly related to crop growth in the red-edge spectral regions [7]. It has been found that the multispectral vegetation indexes based on the red-edge bands are closely related to the physical and chemical parameters of the vegetation [8]. Based on Sentinel-2 multispectral data, this study compared and analyzed the correlations between the multispectral vegetation indexes NDVI, NDVire1, NDVire2, and S2REP and the corn growth parameters (plant height and BBCH). It was found that the NDVI had the lowest correlation with the measured plant height and BBCH when compared with the multispectral vegetation indexes based on the red-edge bands, confirming that the multispectral vegetation indexes based on the red-edge bands are more sensitive to the growth parameters of the corn crop. In addition, the NDVire2 and S2REP indexes calculated by introducing the red-edge 2 band showed better correlations with plant height and BBCH than the NDVire1 index calculated by introducing the red-edge 1 band, which verified that the Sentinel-2 red-edge 2 band has great advantages in monitoring vegetation growth parameters. This result is consistent with the research of Dong et al., who found that introducing the red-edge band to multispectral vegetation indices can effectively improve the estimation accuracy of crop biomass [38]. However, even the red-edge band indexes, which are sensitive to crop growth, only display

the spectral reflectance characteristics at the top of the vegetation canopy. Especially for a corn crop with a large plant size, the optical-based vegetation indexes cannot reflect the internal structural characteristics of the vegetation layer. Therefore, this study investigated a method of estimating corn growth parameters by combining multispectral and backscatter features based on optical and SAR data during the crop growth season.

Compared with optical satellite sensors, Synthetic Aperture Radar (SAR) can obtain internal information on the crop vegetation layer and even soil layer due to its certain penetration ability. Directly using the original backscatter coefficient to estimate crop growth parameters can cause significant errors. This is similar to the research conducted by Baghdadi et al., where SAR signals could penetrate the crops to obtain vegetation and soil information under the crop cover, while directly using the backscatter coefficient for retrieving the soil moisture was not advantageous in presence of a well-developed vegetation cover [39]. However, a radar vegetation scattering model can accurately describe these scattering mechanisms between the vegetation and soil. Among them, the WCM is the most concise and widely used, and is applicable to explain the microwave scattering mechanism in areas with a relatively uniform vegetation coverage such as crop fields [40]. According to the principle of the WCM, the total backscatter received by the radar is related to the vegetation growth parameters (LAI, biomass, etc.) and the surface soil parameters (including surface roughness and soil moisture) [23–25]. Therefore, in this study, based on the WCM theory, we developed a corn crop growth parameter estimation model that combines optical and SAR data without any other external data input. By calculating the difference value  $\Delta\sigma^0$  between the backscatter coefficients of two SAR images synchronized with optical images, it was found that  $\Delta\sigma^0$  weakened the influence of the surface layer on SAR data, revealing the internal structural characteristics of the crop vegetation layer. It also described the differences in radar backscatter coefficient characteristics of a corn crop under the same plant height increment, reflecting the complexity of the vegetation layer structure in a cross-section for different fields. The larger the  $\Delta\sigma^0$  value, the more complex the structural characteristics of the vegetation layer in a unit cross-section, and the larger the LAI or biomass per unit volume of the crop. As Wang et al. proposed, the scattering intensity of vegetation layers increases with the increase in crop LAI [41]. Therefore, in this study, we introduced the DRI into the attenuation coefficient  $\tau^2$  of the WCM to calibrate the optical vegetation indexes  $VI_{opt}$ , and we constructed corn growth parameter estimation models  $VI_{DRI}$ . Essentially, the introduction of radar DRI when constructing the  $VI_{DRI}$  indexes proved to have a better correlation with the corn plant height and BBCH than the use of multispectral indexes  $VI_{opt}$ . Among them, the  $S2REP_{DRI}$  index calculated based on the red-edge 2 band showed the highest estimation accuracy of corn plant height and BBCH phenology, indicating that the  $VI_{DRI}$  indexes constructed based on the WCM principle, combined with the red-edge multispectral vegetation indexes and radar DRI, had certain advantages in improving the estimation accuracy of corn growth parameters. Similarly, based on various regression learning algorithms, David et al. proposed that the combination of optical SAR and optical data can improve the accuracy of vegetation biomass estimation. At the same time, the study found that the Sentinel-2 red-edge 2 band has greater advantages in this regard [42]. However, the existing models were established based on different phenological periods of crops, and the accuracy of the models is difficult to guarantee when the vegetation coverage is high [43,44]. Therefore, this study directly constructed a growth parameter inversion model based on the corn heading phenology, which has important research value for effectively improving the inversion accuracy of a model under a high vegetation coverage.

Additionally, when comparing the estimation results using data from experimental area 1 and experimental area 2, the results showed that the  $VI_{DRI}$  indexes had slightly better accuracy in improving the  $VI_{opt}$  indexes for estimating corn plant height and BBCH in experimental area 1 than in experimental area 2. This is because the SAR images of experimental area 1 were largely synchronized with the optical images, and there was a small interval between the two SAR images. Meanwhile, the interval between the two

SAR images in experimental area 2 was relatively large, and the synchronization between the SAR and optical images was also relatively poor. This indicates that a larger interval between SAR image data will affect the sensitivity of the DRI feature to estimate the crop growth parameters, thereby affecting the accuracy of the  $VI_{DRI}$  model in estimating crop growth parameters. Therefore, in practical applications, the interval between the two SAR images used for calculating DRI should not be too large, and the optical and SAR satellite images should be synchronized as much as possible to ensure that the ground object states observed by the two types of satellites are consistent. In addition, this study found that the  $VI_{DRI}$  indexes have a slightly better accuracy in improving the  $VI_{opt}$  indexes for estimating corn plant height than estimating the BBCH parameter. This is because the plant height reflects the structural characteristics of crops in the vertical direction. SAR data, due to their certain penetrability, can offer insights into the interior of the corn canopy and vertical structural information on the crop. Meanwhile, the phenotypic differences of the corn plant during the tasseling stage are mainly reflected in the extraction status of male spikes at the top of the vegetation canopy, demonstrating the characteristics of two-dimensional plane changes at the top of the corn canopy. This viewpoint is consistent with Caicoya et al., who proposed that SAR features are beneficial for detecting vertical structural information on the vegetation [45]. As such, it seems that the  $VI_{DRI}$  index proposed in this article is more conducive to improving the estimation accuracy of corn plant height compared to the BBCH parameter.

However, the conclusion of this study is mainly based on dual-polarization ( $\sigma^0_{VH}$ ,  $\sigma^0_{VV}$ ) SAR satellite data in the C-band. Beyond these, there are many full-polarization ( $\sigma^0_{VV}$ ,  $\sigma^0_{VH}$ ,  $\sigma^0_{HH}$ ,  $\sigma^0_{HV}$ ) SAR data, and different polarization modes have different abilities in estimating growth parameters of crops. Furthermore, the radar electromagnetic wave scattering characteristics of crop fields vary in different wave bands and polarization modes [2]. Therefore, it is necessary to further verify the applicability of the estimation model in other radar bands and polarization modes. In addition, we mainly studied the corn crops normally planted on the North China Plain. Although we have achieved satisfactory estimation results, due to the limitations of the crop planting region and varieties, additional layout experiments are needed to further verify the universality of the research methods proposed in this paper, by testing them in other corn planting areas such as China's southwest mountainous areas, southern hilly areas, and the Qinghai Tibet Plateau.

## 5. Conclusions

Based on the theory of the vegetation scattering model, in this study, we developed a corn growth parameter estimation model  $VI_{DRI}$  that combines the use of multispectral vegetation indices ( $VI_{opt}$ ) extracted from partially available optical satellite data covering the research area and the differential radar information (DRI) parameter  $\Delta\sigma^0$ , which reflects the internal structural characteristics of the vegetation layer and is only related to the growth status of the crop vegetation. After comparing and analyzing the correlation and parameter estimation accuracies of various multispectral vegetation indexes  $VI_{opt}$  and their corresponding  $VI_{DRI}$  indexes with corn plant height and BBCH phenology, the results indicate that the  $VI_{DRI}$  indexes constructed by combining rich multispectral features from the corn vegetation canopy and SAR features related to the vegetation layer structure show a better correlation with growth parameters. Furthermore, we have found that using a combination of red-edge multispectral and SAR DRI features to construct  $VI_{DRI}$  indexes is advantageous in improving the accuracy of corn growth parameter estimation. This is especially the case for the  $NDVI_{re2_{DRI}}$  and  $S2REP_{DRI}$  indexes constructed in conjunction with the Sentinel-2 satellite data red-edge 2 band, which showed the best correlations with growth parameters compared to the other vegetation indexes.

**Author Contributions:** Conceptualization, Y.W.; methodology, Y.W. and Z.W.; software (MATLAB version R2018a), Y.W.; validation, Y.W., Z.W. and S.L. (Shanjun Luo); formal analysis, Y.W.; investigation, X.H.; resources, X.L.; data curation, S.L. (Shuaibing Liu); writing—original draft preparation, Y.W.; writing—review and editing, Y.W. and Z.W.; visualization, X.L.; supervision, S.L. (Shanjun Luo); project administration, X.H.; funding acquisition, Z.W. All authors have read and agreed to the published version of the manuscript.

**Funding:** This research was supported by the Scientific Research Foundation of the Henan Academy of Sciences (241825013); the Scientific Research Foundation for High-End Talents of the Henan Academy of Sciences (242025005); the Basic Foundation for Scientific Research of the Henan Academy of Sciences (240625002 and 240625003); and the Key R&D projects in Hubei Province (2020BBB058 “Phenomics Research and New Variety Creation of Hybrid rice Based on UAV Remote Sensing”).

**Institutional Review Board Statement:** Not applicable.

**Data Availability Statement:** The dataset used in this paper can be found through the European Space Agency Copernicus Data Space Ecosystem: <https://dataspace.copernicus.eu/>, accessed on 1 September 2021.

**Acknowledgments:** The authors wish to acknowledge the European Space Agency for provision of datasets.

**Conflicts of Interest:** The authors declare no conflict of interest.

## References

- Mandal, D.; Kumar, V.; Ratha, D.; Dey, S.; Rao, Y.S. Dual polarimetric radar vegetation index for crop growth monitoring using sentinel-1 SAR data. *Remote Sens. Environ.* **2020**, *247*, 111954. [CrossRef]
- Wang, H.Q.; Magagi, R.; Goita, K.; Duguay, Y.; Trudel, M.; Muhuri, A. Retrieval performances of different crop growth descriptors from full- and compact-polarimetric SAR decompositions. *Remote Sens. Environ.* **2023**, *285*, 113381. [CrossRef]
- Jia, X.Q.; Feng, M.C.; Yang, W.D.; Wang, C.; Zhang, S. Hyperspectral estimation of aboveground dry biomass of winter wheat based on the combination of vegetation indices. *Chin. J. Ecol.* **2018**, *37*, 424–429.
- Qiao, L.; Tang, W.; Gao, D.; Zhao, R.; An, L.; Li, M.; Sun, H.; Song, D. UAV based chlorophyll content estimation by evaluating vegetation index responses under different crop coverages. *Comput. Electron. Agric.* **2022**, *196*, 106775. [CrossRef]
- Delegido, J.; Verrelst, J.; Meza, C.M.; Rivera, J.P.; Alonso, L.; Moreno, J. A red-edge spectral index for remote sensing estimation of green LAI over agroecosystems. *Eur. J. Agron.* **2013**, *46*, 42–52. [CrossRef]
- Rehman, T.H.; Reis, A.; Akbar, N.; Linnquist, B.A. Use of Normalized Difference Vegetation Index to Assess N Status and Predict Grain Yield in Rice. *Agron. J.* **2019**, *111*, 2889–2898. [CrossRef]
- Dong, T.; Liu, J.; Shang, J.; Qian, B.; Ma, B.; Kovacs, J.M.; Walters, D.; Jiao, X.; Geng, X.; Shi, Y. Assessment of red-edge vegetation indices for crop leaf area index estimation. *Remote Sens. Environ.* **2018**, *222*, 133–143. [CrossRef]
- Bazezew, M.N.; Belay, A.T.; Guda, S.T.; Kleinn, C. Developing Maize Yield Predictive Models from Sentinel-2 MSI Derived Vegetation Indices: An Approach to an Early Warning System on Yield Fluctuation and Food Security. *PFG—J. Photogramm. Remote Sens. Geoinf. Sci.* **2021**, *89*, 535–548. [CrossRef]
- Liu, C.A.; Chen, Z.X.; Shao, Y.; Chen, J.S.; Hasi, T.; Pan, H.Z. Research advances of SAR remote sensing for agriculture applications: A review. *J. Integr. Agric.* **2019**, *18*, 506–525. [CrossRef]
- Romero-Puig, N.; Lopez-Sanchez, J.M. Comparing In-SAR Methodologies for the Retrieval of Paddy Rice Height with TanDEM-X Data. In Proceedings of the IGARSS 2020—IEEE International Geoscience and Remote Sensing Symposium (IGARSS), Waikoloa, HI, USA, 26 September–2 October 2020.
- Yadav, V.P.; Prasad, R.; Bala, R. Leaf area index estimation of wheat crop using modified water cloud model from the time series SAR and optical satellite data. *Geocart. Int.* **2021**, *36*, 791–802. [CrossRef]
- Castillo, J.; Apan, A.A.; Maraseni, T.N.; Salmo, S.G.I. Estimation and mapping of above-ground biomass of mangrove forests and their replacement land uses in the Philippines using Sentinel imagery. *ISPRS J. Photogramm. Remote Sens.* **2017**, *134*, 70–85. [CrossRef]
- Xiuliang, J.; Guijun, Y.; Xingang, X.; Hao, Y.; Haikuan, F.; Zhenhai, L.; Jiachao, S.; Yubin, L.; Chunjiang, Z. Combined Multi-Temporal Optical and Radar Parameters for Estimating LAI and Biomass in Winter Wheat Using HJ and RADARSAR-2 Data. *Remote Sens.* **2015**, *7*, 13251. [CrossRef]
- Luo, P.; Liao, J.J.; Shen, G.Z. Combining Spectral and Texture Features for Estimating Leaf Area Index and Biomass of Maize Using Sentinel-1/2, and Landsat-8 Data. *IEEE Access* **2020**, *8*, 53614–53626. [CrossRef]
- Abdikan, S.; Sekertekin, A.; Narin, O.G.; Delen, A.; Sanli, F.B. A comparative analysis of SLR, MLR, ANN, XGBoost and CNN for crop height estimation of sunflower using Sentinel-1 and Sentinel-2. *Adv. Space Res.* **2023**, *71*, 3045–3059. [CrossRef]

16. Yeasin, M.; Haldar, D.; Kumar, S.; Paul, R.K.; Ghosh, S. Machine Learning Techniques for Phenology Assessment of Sugarcane Using Conjunctive SAR and Optical Data. *Remote Sens.* **2022**, *14*, 3249. [[CrossRef](#)]
17. Tao, L.; Li, J.; Jiang, J.; Chen, X. Leaf Area Index Inversion of Winter Wheat Using RADARSAT-2 Data and Modified Water cloud Model. *J. Triticeae Crops* **2016**, *36*, 236–242.
18. Bao, Y.; Zhang, Y.; Wang, J.; Min, J. Surface soil moisture estimation over dense crop using Envisat ASAR and Landsat TM imagery: An approach. *Int. J. Remote Sens.* **2014**, *35*, 6190–6212. [[CrossRef](#)]
19. Davitt, A.; Winter, J.M.; McDonald, K. Integrated crop growth and radiometric modeling to support Sentinel synthetic aperture radar observations of agricultural fields. *J. Appl. Remote Sens.* **2020**, *14*, 044508. [[CrossRef](#)]
20. Ramesh, N.; Heiko, B.; Kevin, T.; Keith, M.; Sarah, J.; France, G.; Charles, G.; Yadvinder, M.; Geoff, B.; Sam, D.; et al. Airborne S-Band SAR for Forest Biophysical Retrieval in Temperate Mixed Forests of the UK. *Remote Sens.* **2016**, *8*, 609. [[CrossRef](#)]
21. Zhang, H.B.; Wang, C.C.; Zhu, J.J.; Fu, H.Q.; Han, W.T.; Xie, H.Q. Forest Aboveground Biomass Estimation in Subtropical Mountain Areas Based on Improved Water Cloud Model and PolSAR Decomposition Using L-Band PolSAR Data. *Forests* **2023**, *14*, 2303. [[CrossRef](#)]
22. Dave, R.; Saha, K.; Kushwaha, A.; Pandey, D.K.; Vithalpur, M.; Parath, N.; Murugesan, A. Application of sentinel-1 SAR-derived vegetation descriptors for soil moisture retrieval and plant height prediction during the wheat growth cycle. *Int. J. Remote Sens.* **2023**, *44*, 786–801. [[CrossRef](#)]
23. Yang, Z.; Li, K.; Shao, Y.; Brisco, B.; Liu, L. Estimation of Paddy Rice Variables with a Modified Water Cloud Model and Improved Polarimetric Decomposition Using Multi-Temporal RADARSAT-2 Images. *Remote Sens.* **2016**, *8*, 878. [[CrossRef](#)]
24. Kweon, S.K.; Oh, Y.A. Modified Water-Cloud Model with Leaf Angle Parameters for Microwave Backscattering from Agricultural Fields. *IEEE Trans. Geosci. Remote Sens.* **2015**, *53*, 2802–2809. [[CrossRef](#)]
25. Bai, X.; He, B.; Li, X.; Zeng, J.; Wang, X.; Wang, Z.; Zeng, Y.; Su, Z. First Assessment of Sentinel-1A Data for Surface Soil Moisture Estimations Using a Coupled Water Cloud Model and Advanced Integral Equation Model over the Tibetan Plateau. *Remote Sens.* **2017**, *9*, 714. [[CrossRef](#)]
26. Ahmadian, N.; Ullmann, T.; Verrelst, J.; Borg, E.; Conrad, C. Biomass Assessment of Agricultural Crops Using Multi-temporal Dual Polarimetric TerraSAR-X Data. *PFG—J. Photogramm. Remote Sens. Geoinf. Sci.* **2019**, *87*, 159–175. [[CrossRef](#)] [[PubMed](#)]
27. Chauhan, S.; Srivastava, H.S.; Patel, P. Crop Height Estimation Using RISAT-1 Hybrid Polarized Synthetic Aperture Radar Data. *IEEE J. Sel. Top. Appl. Earth Obs. Remote Sens.* **2019**, *12*, 2928–2933. [[CrossRef](#)]
28. Bleiholder, H.; Kirfel, H.; Langeluddeke, P.; Stauss, R.; Van, D.B.T. A Uniform Code for the Phenological Stages of Crops and Weeds. *Pesqui. Agropecu. Bras.* **1991**, *26*, 1423–1429.
29. Zadoks, J.C.; Chang, T.T.; Konzak, C.F. A decimal code for the growth stages of cereals. *Weed Res.* **1974**, *14*, 415–421. [[CrossRef](#)]
30. QX/T 361-2016; Specification for Agricultural Meteorological Observation Maize. China Meteorological Administration: Beijing, China, 2016.
31. Wang, Y.; Fang, S.; Zhao, L.; Huang, X. Estimation of maize plant height in North China by means of backscattering coefficient and depolarization parameters using Sentinel-1 dual-pol SAR data. *Int. J. Remote Sens.* **2022**, *43*, 1960–1982. [[CrossRef](#)]
32. Rouse, J.W.; Haas, R.H.; Schell, J.A.; Deering, D.W. Monitoring Vegetation Systems in the Great Plains with ERTS. *NASA Spec. Publ.* **1974**, *351*, 309.
33. Fernandez-Manso, A.; Fernandez-Manso, O.; Quintano, C. SENTINEL-2A red-edge spectral indices suitability for discriminating burn severity. *Int. J. Appl. Earth Obs. Geoinf.* **2016**, *50*, 170–175. [[CrossRef](#)]
34. Mercier, A.; Betbeder, J.; Baudry, J.; Roux, V.L.; Hubert-Moy, L. Evaluation of Sentinel-1 & 2 time series for predicting wheat and rapeseed phenological stages. *ISPRS J. Photogramm. Remote Sens.* **2020**, *163*, 231–256.
35. Attema, E.; Ulaby, F.T. Vegetation modeled as a water cloud. *Radio Sci.* **1978**, *13*, 357–364. [[CrossRef](#)]
36. Lievens, H.; Verhoest, N. On the Retrieval of Soil Moisture in Wheat Fields from L-Band SAR Based on Water Cloud Modeling, the IEM, and Effective Roughness Parameters. *IEEE Geosci. Remote Sens. Lett.* **2011**, *8*, 740–744. [[CrossRef](#)]
37. Kokhan, S.; Vostokov, A. Using Vegetative Indices to Quantify Agricultural Crop Characteristics. *J. Ecol. Eng.* **2020**, *21*, 120–127. [[CrossRef](#)] [[PubMed](#)]
38. Dong, T.; Meng, J.; Shang, J.; Liu, J.; Wu, B. Evaluation of Chlorophyll-Related Vegetation Indices Using Simulated Sentinel-2 Data for Estimation of Crop Fraction of Absorbed Photosynthetically Active Radiation. *IEEE J. Sel. Top. Appl. Earth Obs. Remote Sens.* **2015**, *8*, 4049–4059. [[CrossRef](#)]
39. Baghdadi, N.; El Hajj, M.; Zribi, M.; Bousbih, S. Calibration of the water cloud model at C-Band for winter crop fields and grasslands. *Remote Sens.* **2018**, *9*, 13. [[CrossRef](#)]
40. Li, J.H.; Wang, S.S. Using SAR-Derived Vegetation Descriptors in a Water Cloud Model to Improve Soil Moisture Retrieval. *Remote Sens.* **2018**, *10*, 1370. [[CrossRef](#)]
41. Wang, R.; Chen, J.M.; He, L.M.; Liu, J.E.; Shang, J.L.; Liu, J.G.; Dong, T.F. A novel semi-empirical model for crop leaf area index retrieval using SAR co- and cross-polarizations. *Remote Sens. Environ.* **2023**, *296*, 113727. [[CrossRef](#)]
42. David, R.M.; Rosser, N.J.; Donoghue, D.N.M. Improving above ground biomass estimates of Southern Africa dryland forests by combining Sentinel-1 SAR and Sentinel-2 multispectral imagery. *Remote Sens. Environ.* **2022**, *282*, 113232. [[CrossRef](#)]
43. Gao, S.; Niu, Z.; Huang, N.; Hou, X. Estimating the Leaf Area Index, height and biomass of maize using HJ-1 and RADARSAT-2—ScienceDirect. *Int. J. Appl. Earth Obs. Geoinf.* **2013**, *24*, 1–8.

44. Hosseini, M.; Mcnairn, H.; Mitchell, S.; Robertson, L.D.; Davidson, A.; Homayouni, S. Integration of synthetic aperture radar and optical satellite data for corn biomass estimation. *Methodsx* **2020**, *7*, 100857. [[CrossRef](#)] [[PubMed](#)]
45. Caicoya, A.T.; Kugler, F.; Pardini, M.; Hajnsek, I.; Papathanassiou, K. Vertical forest structure characterization for the estimation of Above Ground Biomass: First experimental results using SAR vertical reflectivity profiles. In Proceedings of the IEEE Joint International Geoscience and Remote Sensing Symposium (IGARSS)/35th Canadian Symposium on Remote Sensing, Quebec City, QC, Canada, 13–18 July 2014.

**Disclaimer/Publisher's Note:** The statements, opinions and data contained in all publications are solely those of the individual author(s) and contributor(s) and not of MDPI and/or the editor(s). MDPI and/or the editor(s) disclaim responsibility for any injury to people or property resulting from any ideas, methods, instructions or products referred to in the content.